ARMY RESEARCH LABORATORY

Environment and Circuit Model for Capacitor-Based Rail Guns

by William Coburn, Ira Kohlberg,
Warren Williams, and Calvin Le

ARL-TN-46

April 1995

The findings in this report are not to be construed as an official Department of the Army position unless so designated by other authorized documents.

Citation of manufacturer's or trade names does not constitute an official endorsement or approval of the use thereof.

Destroy this report when it is no longer needed. Do not return it to the originator.

REPORT DOCUMENTATION PAGE

Form Approved
OMB No. 0704-0188

1. AGENCY USE ONLY *(Leave blank)*	2. REPORT DATE	3. REPORT TYPE AND DATES COVERED
	April 1995	Final, from May to September 1994

4. TITLE AND SUBTITLE
Environment and Circuit Model for Capacitor-Based Rail Guns

5. FUNDING NUMBERS
PE: 61102

6. AUTHOR(S)
William Coburn (ARL), Ira Kohlberg (Kohlberg Assoc.), Warren Williams (ARDEC), and Calvin Le (ARL)

7. PERFORMING ORGANIZATION NAME(S) AND ADDRESS(ES)
U.S. Army Research Laboratory
Attn AMSRL-WT-ND
2800 Powder Mill Road
Adelphi, MD 20783-1197

8. PERFORMING ORGANIZATION REPORT NUMBER
ARL-TN-46

9. SPONSORING/MONITORING AGENCY NAME(S) AND ADDRESS(ES)
U.S. Army Research Laboratory
2800 Powder Mill Road
Adelphi, MD 20783-1197

10. SPONSORING/MONITORING AGENCY REPORT NUMBER

11. SUPPLEMENTARY NOTES
AMS code: 611102H430011
ARL PR: 4EE3E3

12a. DISTRIBUTION/AVAILABILITY STATEMENT
Approved for public release; distribution unlimited.

12b. DISTRIBUTION CODE

13. ABSTRACT *(Maximum 200 words)*

High-power electromagnetic devices such as rail guns require pulse power systems that can generate peak powers between 10^8 and 10^{11} W and generate electromagnetic fields whose dominant energy spectrum falls between quasi-dc and tens of kilohertz. These fields may be important for electromagnetic compatibility (EMC), and may also be of concern for environmental and biological effects. This paper summarizes the results of the first phase of a U.S. Army Research Laboratory program that deals with the characterization of the electromagnetic fields produced by laboratory rail guns, the results of which can be scaled to operational size systems. Included are discussions of the pulsed power system, measurement techniques, theoretical models, and selected experimental data.

14. SUBJECT TERMS
EM fields, EM launch

15. NUMBER OF PAGES
15

16. PRICE CODE

17. SECURITY CLASSIFICATION OF REPORT	18. SECURITY CLASSIFICATION OF THIS PAGE	19. SECURITY CLASSIFICATION OF ABSTRACT	20. LIMITATION OF ABSTRACT
Unclassified	Unclassified	Unclassified	UL

NSN 7540-01-280-5500

Standard Form 298 (Rev. 2-89)
Prescribed by ANSI Std. Z39-18
298-102

Contents

Figures

1. Introduction

Electromagnetic (EM) launchers such as rail guns (see fig. 1) are relatively new devices for generating hypervelocity projectiles. As indicated in figure 1, the projectile is accelerated between the rails by the $I \times B$ force until it exits at the muzzle. The magnetic induction, B, is created by the current in the rails, and I is the loop current flowing through the rails and armature. Although the acceleration issues concerning these devices have been studied for some time, the electromagnetic compatibility (EMC) issues related to their integration into a system have only recently been examined [1]. This report addresses the salient features of the EM environment under live-fire conditions, discusses the instrumentation and techniques used to measure the electric (E-) and magnetic (H-) fields, describes the representation and modeling of this inherently nonlinear device as a circuit element, and compares theoretical predictions of the fields with selected experimental results. The emphasis of this report is to provide an overview of the EMC issues that are relevant to these high-power electromagnetic (HPEM) devices. The two-rail gun in figure 1 has dimensions l = 1 m, w = 15 mm, h = 19 mm, and d = 10 mm, is contained by a laminated steel barrel, and is powered by a capacitor bank to produce peak rail currents up to 160 kA. In our experiments, projectile acceleration was not an issue, so nine firings of a solid armature were used as a test bed for EM field measurements. Previous reports [2–6] provide detailed information on all aspects of the experiments. A typical H-field measured near a two-turn, series-augmented rail gun 1 m long with a laminated steel barrel is also shown for comparison. Extending the theoretical model to include variations in the rail gun design is currently under investigation.

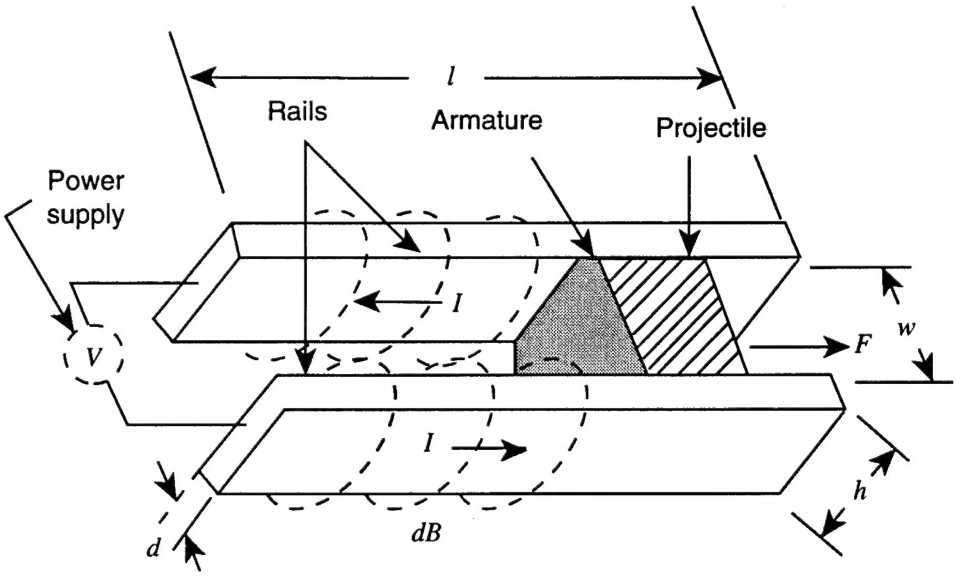

Figure 1. Rail gun and coordinate system.

2. Pulse Power System and Rail Current

In the absence of friction or other losses, the equation of motion of the armature is

$$m \frac{d^2 z_A}{dt^2} = \frac{1}{2} L_e' I^2 , \tag{1}$$

where m is the combined armature-plus-projectile mass, $z_A(t)$ is the position of the armature, and L_e' is a theoretically derived "effective" inductance gradient that takes into account the transmission-line inductance per unit length of the rails and the efficiency of magnetic field force coupling to the armature [2,3]. When equation (1) is combined with the rail-gun driving circuit of figure 2 and the transmission-line model for the rails [2-4], a system of nonlinear time-dependent equations is developed whose solution provides the transient current and associated EM fields.

The rails are connected to the four capacitor banks shown in figure 2. Although not indicated, diodes are placed across the capacitors to prevent reverse current. The load resistor, R_L = 100 Ω, is sufficiently large to allow a measure of the muzzle voltage. Since the main function of this initial phase of the program was to characterize the rail-gun EM environment, it was sufficient to simply measure the rail current in order to verify our theoretical model for the rail-gun inductance [7,8], the efficiency of coupling to the armature [2–4], and the computation of the fields from the current [1–6]. The measured rail current is well approximated by the expression

$$I(t) = 190\left(e^{-500t} - e^{-13{,}000t}\right) \text{kA} . \tag{2}$$

This current has a peak amplitude of 160 kA with a risetime of about 300 μs. It is this expression that is used in equation (1) to compute the armature velocity and acceleration.

The electrical model of a rail gun with augmenting turns is modified to include the series inductance and resistance of the augmenting rails and cross-over connections. For our purposes, variations in the pulse power system are not important as long as the rail current can be adequately characterized. However, the rail-gun inductance gradient must be known accu-

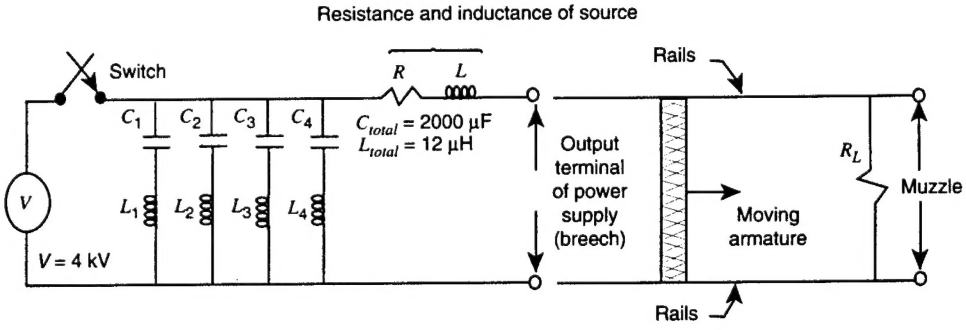

Figure 2. Rail-gun electrical model.

rately, including the mutual inductance between the primary and secondary rails. The determination of the "effective" inductance gradient for use in equation (1) is an area of current research.

3. Electromagnetic Field Measurements

The H-field time derivative ($\dot{H}$) is measured with a 13.3-cm-diameter, 36-turn coil, which responds to the field component normal to the coil. These sensors have a bandwidth of 30 Hz to 100 kHz, with a low-pass filter to exclude the sensor resonance. As shown elsewhere [5], the sensor voltage is a good measure of $\dot{H}$ in this frequency range, so the H-field can be obtained by numerical integration. H-field measurements at radial distances from 5 cm to 1 m were conducted at several locations along the length of the barrel. We obtained E-field measurements using Stanford Research Institute E-field sensors, which are a top-loaded monopole antenna design. The sensor is calibrated to include the effect of being mounted on a metal canister. The sensor bandwidth is 2 kHz to 200 MHz, so the acquired data are corrected according to the known sensor response as a function of frequency. E-field data were limited because of instrumentation failures and were obtained only near the breech and muzzle.

The measurement instrumentation includes digital storage oscilloscopes and the various data acquisition components. The $\dot{H}$ data are acquired through shielded coaxial cable. E-field data are acquired through a fiber-optic data link, which provides attenuation or amplification and has a bandwidth of 45 Hz to 200 MHz. Noise measurements verified an adequate signal-to-noise ratio for the various measurement systems. The acquired data are corrected for linear scale factors and stored in digitized form. $\dot{H}$ measurements are numerically integrated in the time domain. E-field measurements require frequency-domain correction for the probe response, which is done numerically in the Fourier transform space with the transient data obtained by Fourier inversion.

4. Comparison Between Theory and Experiment

The starting point for predicting the time-dependent H-field is the determination of the position of the armature, $z_A(t)$, as computed from equation (1). As shown elsewhere [3], the effective inductance gradient, L'_e, is given by

$$L'_e = E_0 L'_r \quad , \tag{3}$$

where L'_r is the inductance gradient of the rails and E_0 is a theoretically derived EM efficiency factor that accounts for the leakage of the H-field over the area external to the armature. To a first approximation, the inductance gradient is simply the rail-gun inductance per unit length. From the parallel-plate transmission-line model of Baum et al [7], the predicted rail inductance gradient of L'_r = 0.52 μH/m compared very well with the

measured value of 0.522 μH/m. Application of the simplified theory of a microstrip transmission line developed elsewhere [8] to the rail-gun configuration provides a value of $E_0 = 0.75$ [2,3]. This produces an effective inductance gradient of 0.39 μH/m.

Using the current of equation (2), the value $L'_e = 0.39$ μH/m, and 11 g for the armature mass provides both the velocity and position of the armature as a function of time. The first integral of equation (1) gives the velocity, $v(t)$, and the second integral, $z_A(t)$. Figure 3 shows a comparison between the measured velocity (averaged over eight shots) and predicted results. The anomalies near muzzle exit are repeatable and may be attributable to contact arcing. Figure 4 shows a comparison between the measured and calculated armature positions as a function of time. The armature starts at 2.5 cm, which is not included in the model, but otherwise the agreement is quite good.

Because of the low frequencies (long wavelengths), the Biot-Savart law is sufficient for computing the time-dependent H-field. If the distance of the observation point from the bore center is comparable to the dimensions and separation of the rails, the spatial distribution of the current along the

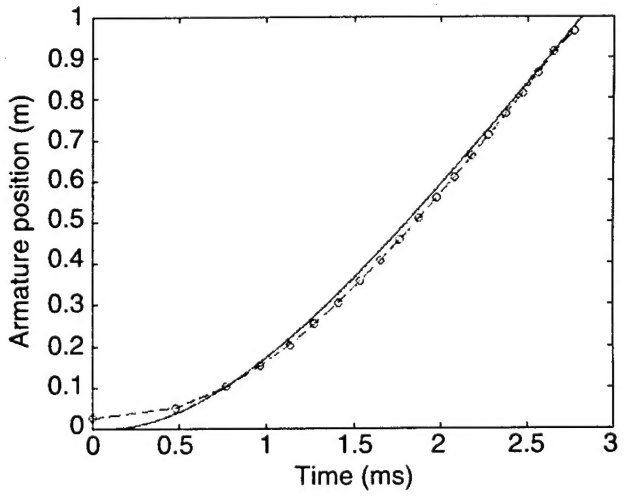

Figure 3. Measured armature velocity (dashed line) versus theory (solid line) for $E_0 = 0.75$.

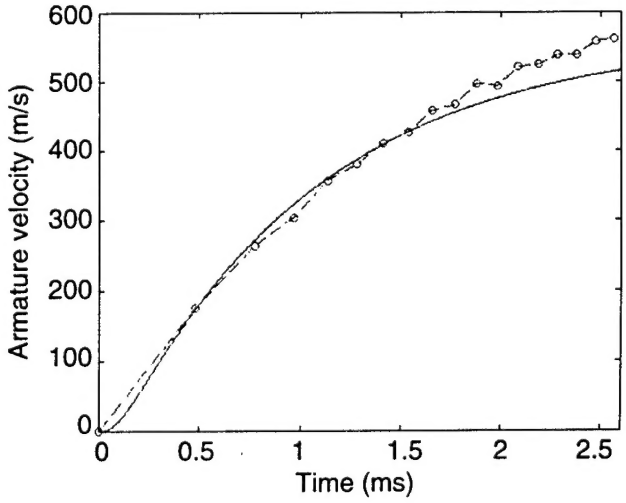

Figure 4. Measured armature position (dashed line) versus theory (solid line) for $E_0 = 0.75$.

rails and armature must be taken into account [2]. When the observation points are much greater than the rail height and rail width, the detailed spatial distribution of current is not important, and the current along the rails can be treated as filaments. This latter condition is applicable to our experiments, since the closest measurement locations are 5 cm from center bore.

Figure 5 shows a comparison between the experimental and theoretical behavior of the vertical component of the *H*-field in the plane of symmetry (i.e., between the rails) at 5 cm above the rails and 71 cm from the breech. Note that the field peaks when the armature passes the probe location and decays abruptly after muzzle exit, so that the initial time delay and the waveform pulse width depend on the observation point. The agreement for this case is good; however, we noticed that as the distance of the observation point from the bore center increased, the discrepancy between the amplitude of the theoretical and experimental curves increased, with the experimental values being larger. The temporal shape of the experimental curves, however, remained consistent with the results shown in figure 5. Closer examination of the *H*-field components indicates that the vector nature of the field changes as the distance from the bore center increases. This behavior may be attributable to metal structures surrounding the rail gun and would not be predicted in the free-space model of the rails.

These preliminary findings may indicate the existence of a parasitic or anomalous current flowing somewhere in the laboratory that was driven by the power supply. Such anomalous currents would not produce *H*-fields near the rails that were significant to those produced by the rail current. They could, however, produce *H*-fields comparable to those produced by the rails at greater distances (consistent with our observation points).

An example of the *B*-field ($B = \mu_0 H$) in the plane of symmetry of a 1.2-m, two-turn, series-augmented gun is presented for comparison. The vertical component is shown in figure 6 at roughly 20 cm above and 61 cm from the breech. The peak rail current is about 350 kA, with temporal behavior

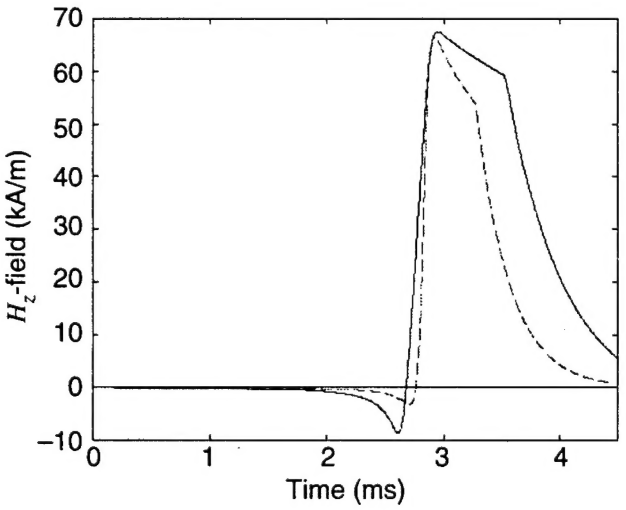

Figure 5. Comparison between experimental (solid line) and theoretical (dashed line) behavior of vertical *H*-field in symmetry plane at 5 cm above and 71 cm from breech.

similar to that given by equation (2). The peak B-field (678 gauss or 678×10^{-4} tesla) associated with the two-turn rail gun is on the same order as for the single-turn gun (for equivalent rail current). However, the waveform is different where the second peak is related to the muzzle cross-over connection. Contributions from the current in the rails and buswork can be readily seen in the transient waveform depending on the observation point. Preliminary modeling has shown that to obtain reasonable agreement for the transient fields, we need filament models for the cross-over connections that carry current at the appropriate times.

In addition to H-field measurements, we obtained a limited number of E-field measurements near the single-turn rail gun. The most interesting of these appeared near the muzzle, where the effects of arcing produced high-frequency components. Figure 7 shows a representative measured field near the muzzle. The horizontal component (i.e., across the rails) is measured at two heights above the muzzle. The initial spike is associated with switching transients, while muzzle exit occurs at about 2.5 ms with additional arcing afterwards. As can be seen in figure 7, the initial spike and the transmission-line fringing fields do not fall with distance as fast as the arcing contributions, as in the near-field of a dipole radiator. The effects of this type of field on nearby electronic equipment remain to be explored.

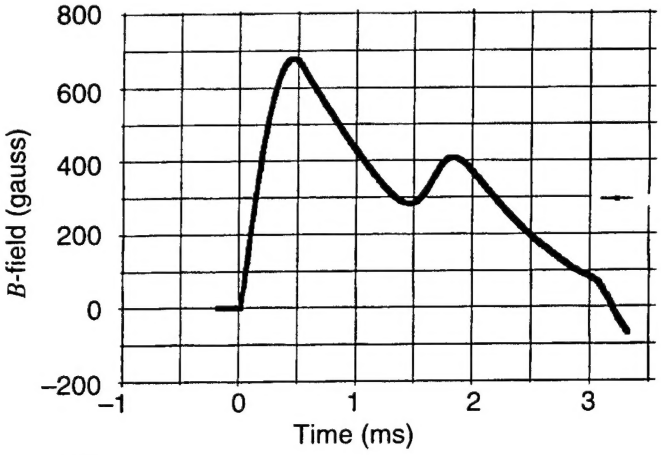

Figure 6. Vertical B-field in symmetry plane at 20 cm above and 61 cm from breech.

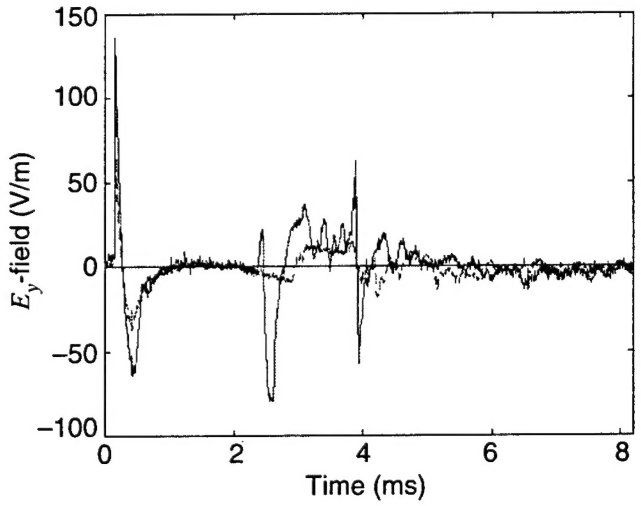

Figure 7. Measured E_y-field at 20 cm (solid line) and 41 cm (dashed line) above muzzle.

5. Conclusion

Predictions of the muzzle exit velocity for the two-rail gun, based on our theoretical model for the rail-gun inductance gradient, are within 5 percent of the experimental data. This verifies that the "effective" inductance gradient is the important theoretical quantity and validated our approach to determining the efficiency factor. Extending our approach to more complicated rail-gun designs is currently under investigation.

Comparisons between calculated and measured magnetic fields show good agreement close to the rails. Discrepancies appear for observation points more than about 0.3 m from the bore, and we are in the process of resolving this issue. It is believed that the vector nature of the field is altered owing to the presence of nearby metal structures, which is not accounted for in the free-space model of the rail gun. For all observation points, specific features of the transient waveform can be readily identified and related to the armature dynamics. This is also true for augmented rail guns, but the filament current model becomes more complicated. In this case the primary rails, secondary rails, and cross-over connections must carry current at the appropriate time according to the armature dynamics.

The large magnetic fields produced by these HPEM devices require that we consider electromagnetic interference/compatibility (EMI/EMC) issues to ensure compatibility with other electronic equipment. Mitigation techniques such as shielding or separation would typically be required. Shielding issues must necessarily be considered an integral part of the rail-gun design, because they have a direct impact on the "effective" inductance gradient of the rail gun. This in turn influences the size of the system and the terminal projectile velocity. The rail-gun barrel provides physical containment and support for the rails and is typically designed to prevent induced eddy currents. The laminated steel barrels considered here provide little shielding and so are not included in the theoretical models. The presence of materials designed to provide magnetic shielding must be included in the calculation of the transmission-line inductance per unit length. Shielding solutions would also affect the efficiency of the force coupling to the armature and are an area of current research.

Acknowledgments

The authors would like to acknowledge the instrumental support of the ARL Transonic Range staff and management. We would like to thank Alex Zielinski and staff of the EM Gun Facility for making these experiments possible.

References

1. M. L. Haberman, *EMI/EMC Issues Associated with Rail Guns*, Department of Defense Electromagnetic Compatibility Analysis Center, ECAC-CR-93-086 (November 1993).

2. I. Kohlberg, *Prediction of Electromagnetic Fields Generated by Rail Guns*, Kohlberg Associates, Inc., Final Report to Battelle, Prime Contract DAALO3-91-C-0034, Subcontract No. 93419 (March 1994).

3. I. Kohlberg and W. O. Coburn, *A Solution for the Three-Dimensional Rail Gun Current Distribution and Electromagnetic Fields of a Rail Launcher*, IEEE Trans. Magn. **31**, No. 1 (January 1995), pp 628–633.

4. I. Kohlberg and W. O. Coburn, *Theoretical and Experimental Investigation of Electromagnetic Fields Generated by Rail Guns*, Proceedings of the 12th International Wroclaw Symposium and Exhibition on Electromagnetic Compatibility, Wroclaw, Poland (28 June–1 July 1994).

5. W. O. Coburn, C. Le, D. DeTroye, G. Blair, and W. Williams, *Electromagnetic Field Measurements Near a Rail Gun*, IEEE Trans. Magn. **31**, No. 1 (January 1995), pp 698–703.

6. W. O. Coburn and W. Williams, *Static and Quasi-static Models for the Magnetic Field of a Rail Gun*, IEEE Trans. Magn. **31**, No. 1 (January 1995), pp 692–697.

7. C. E. Baum, D. V. Giri, and R. D. Gonzalez, *Electromagnetic Field Distribution of the TEM Mode in a Symmetrical Two-Parallel-Plate Transmission Line*, Air Force Weapons Laboratory, Sensor and Simulation Note 219 (April 1976).

8. F. Assadourian and F. Rimai, *Simplified Theory of Microstrip Transmission Systems*, Proc. IRE **40** (1952), 1651.

Distribution

Admnstr
Defns Techl Info Ctr
Attn DTIC-DDA (2 copies)
Cameron Sta Bldg 5
Alexandria VA 22304-6145

Director
Defns Intllgnc Agcy
Attn RTS-2A Techl Lib
Washington DC 20301

Defns Nuc Agcy
Attn RAES Elect Syst Techlgy Div
Attn RAST Electromagnetic Applctn Div
Attn TITL Tech Lib
6801 Telegraph Rd
Alexandria VA 22310-3398

Defs Nuc AgencyOffice of Techl Applications
Attn D R Lewis
Alexandria VA 22310

Commander
Atmospheric Sci Lab
Attn STEWS-NE J Meason
White Sands Missile Range NM 88002-5180

Ofc of the Assist Secy of the Army
for Rsrch Dev & Acqstn
Attn SARD-TR Dr R Chait
Room 3E476 The Pentagon
Washington DC 20310-0103

Cmdr
US Army ARDEC
Attn AMSTA-AR-CCL-D W Williams
(3 copies)
Attn SMCAR-AEC-IE N Svendsen
Bldg 65 N
Picatinny Arsenal NJ 07806-5000

US Army AVRDEC
Attn AMSAT-R-EFM P Haselbauer
4300 Goodfellow Blvd
ST Louis MO 63120-1798

US Army BRDEC
Attn SATB-FGE J Ferrick
Attn SATB-FGE T Childers
FT Belvoir VA 22060-5606

Commander
US Army Matl Cmnd
Attn AMCAM-CN
5001 Eisenhower Ave
Alexandria VA 22333-0001

Director
US Army Mis Cmnd (USAMICOM)
Attn AMSMI-RD-CS-R Documents
Redstone Arsenal AL 35898-5400

Cmdr
US Army MRDEC
Attn AMSMI-RD-ST-CM J Vandier
Huntsville AL 35898-5240

US Army Natick RDEC
Attn SATNC-SUSD-SHD A Murphy
Kansas Stret
Natick MA 01760-5018

Commander
US Army Nuc & Chem Agcy
Attn MONA-NU R Pfeffer
7150 Heller Loop Rd Ste 101
Springfield VA 22150

Cmdr
US Army TARDEC
Attn AMSTA-ZT G Baker
Warren MI 48397-5000

Commander
US Army TECOM
Attn STERT-TE-E J Knaur
Redstone Technical Test Center
Huntsville AL 35898-8052

US Army TECOM Techl Dir Ofc
Attn AMSTE-TC-D R Bell
Aberdeen Proving Ground MD 21005

Distribution

Nav Rsrch Lab
Attn Code 4820 Techl Info Div
4555 Overlook Ave SW
Washington DC 20375-5000

Commander
Nav Surfc Weapons Ctr
Attn Code E231 Techl Lib
Dahlgren VA 22448-5020

Nav Warfare Ctr
Attn Code OZT T Conway
Lakehurst NJ 08733

Dir Air Force Armament Directorate
Attn WL/MNAA S Federle
101 W Eglin Blvd. Ste 346A
Eglin AFB FL 32542-6810

Natl Inst of Stand & Techlgy
Attn V Ulbrecht Rsrch Info Ctr
Rm E01 Bldg 101
Gaithersburg MD 20899

DoD Joint Spectrum Center
Attn CA J Word (3 copies)
120 Worthing Basin
Annapolis MD 21401

US Army Rsrch Lab
Aberdeen Proving Ground
Attn AMSRL-WT-PB Chf
Attn AMSRL-WT-WB Chf
Attn AMSRL-WT-WC Chf
Attn AMSRL-WT-WD Chf

US Army Rsrch Lab
Adelphi Center
Attn AMSRL-OP-SD-TA Mail & Records Mgmt
Attn AMSRL-OP-SD-TL Tech Library (3 copies)
Attn AMSRL-OP-SD-TP Tech Pub
Attn AMSRL-SS-F Chf
Attn AMSRL-SS-S Chf
Attn AMSRL-WT-N Chf
Attn AMSRL-WT-NB Chf
Attn AMSRL-WT-ND C Le (5 copies)
Attn AMSRL-WT-ND Chf
Attn AMSRL-WT-ND W O Coburn (3 copies)
Attn AMSRL-WT-NE Chf
Attn AMSRL-WT-NF Chf
Attn AMSRL-WT-NG Chf
Attn AMSRL-WT-NH Chf
Attn AMSRL-WT-NJ Chf
Attn AMSRL-WT-N Sr Rsrch Scntst
Attn AMSRL-WT-ND J Latess